A Model of Interfacial Permeability for Soft Seals in Marine-Organism, Suction-Based Adhesion

Michael Beckert[1], Brooke E. Flammang[2] and Jason H. Nadler[1]
[1]Georgia Tech Research Institute Advanced Concepts Laboratory
Atlanta, GA 30318, U.S.A.
[2]New Jersey Institute of Technology Department of Biological Sciences,
Newark, NJ, 07102, U.S.A.

ABSTRACT

Reversible, suction based adhesion employed by many marine organisms may provide unique, adaptable technologies for biologically inspired grasping devices that function in difficult submerged environments. Here a theoretical framework based on measurable structural, material, and topological properties is developed to better understand a critical aspect of suction based attachment strategies: the leakage rate. The utility of the approach is demonstrated on an experimental apparatus designed to mimic the flow conditions experienced by a suction-based attachment device. Furthermore, the sealing effectiveness of a remora fish on sharkskin is investigated as a biological example.

INTRODUCTION

Controlling fluids with proper seal and joint design has long been a topic of interest in engineering [1], and traditionally creating a proper seal that minimizes leakage requires such considerations as stiff mating members with smooth finished surfaces and adequate compression of the gasket material [2]. In natural marine environments, fluid management by the use seals occurs with the added difficulty that surface topology may be rough and uneven [3, 4]. Despite these considerations, many organisms are capable of forming robust seals against these challenging surfaces using their soft tissues and attachment structures without large compressive loads as part of their reversible attachment strategy. Cephalopods [5, 6], remora (family Echeneidae) [7], lumpsuckers (family Cyclopteridae) [8, 9], river loaches (family Balitoridae) [10] and clingfish (family Gobiesocidae) [3, 4] are examples of organisms that accomplish reversible attachment by sealing off a localized region of sub-ambient pressure between themselves and a surface. The ability of these organisms to create a seal is critical to their attachment strategy because without it, the reduced pressure that facilitates the suction-based attachment force cannot be maintained. In this work, a multi-scale model is implemented to predict leakage across a soft seal in contact with a rough mating surface based on the surface's topology, the mechanical properties of the soft seal, and the rheological properties of the surrounding fluid. Such a model is useful for analyzing the sealing performance of natural tissues and structures, but also for seeking manmade materials and designs to mimic the animals' behavior.

The primary concern in any sealing application is the elimination of flow channels across the seal where leakage occurs. These channels commonly develop on rough sealing surfaces from local asperities that form gaps at the interface [11, 12]. Consider the suction pad of a remora fish (Figure 1a). By pressing its suction pad against a host, the remora is able to create a robust suction seal against a multitude of surfaces both natural and artificial including sharks, rays, other pelagic fish, sea turtles, dolphins, divers, buoys, ship hulls, and concrete [13-20]. The

perimeter of the suction pad is formed by soft tissue known as the fleshy lip (Figure 1a and b) which is responsible for the suction seal [21, 22]. Tissue structures in other organisms have similar functions including modified pelvic fins of clingfish [3] and lumpsuckers [8], modified ventral fins of river loaches [10] or sucker arrays in cephalopods [6, 23]. Figure 1c shows a cross-sectional schematic of the remora fleshy lip in contact with a rough substrate. During attachment as the soft tissue conforms to the attachment site (Figure 1d), sub-ambient pressure inside the pad causes fluid leakage across the seal [24, 25]. In order to maintain adhesion, leakage into the pad must be minimized as it ultimately eliminates the pressure difference due to the finite volume of the organism's attachment structures (i.e. eventually tissues will be stretched to their limit as the attachment structure fills with fluid and eventually rendered unable to maintain sub-ambient pressures).
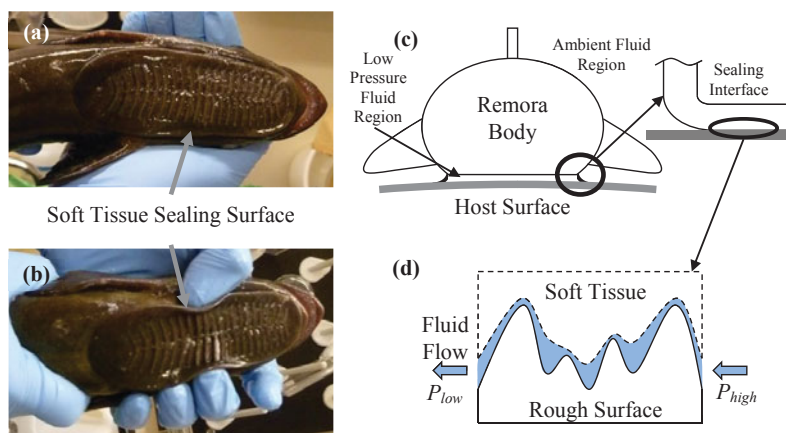

Figure 1. (a, b) Remora (*Echeneis naucrates*) dorsal suction pad, **(c)** macro-scale cross-sectional schematic of soft tissue and sealing interface, **(d)** micro-scale schematic of fluid flow through gaps between soft tissue and rough surface

Although prolonged attachment is beneficial to the remora [19] and other organisms utilizing suction, previous work has often evaluated attachment structures with respect to the maximum, near-instantaneous pull-off force the organism can endure without addressing other aspects of performance such as sealing effectiveness [3, 7, 8]. While the maximum pull-off force provides vital information as to an organisms' ability to withstand large disruptive forces, it does not provide information relevant to other difficult conditions such as long attachment periods to rough surfaces under low to moderate loads (e.g. potentially arising from fluid drag due to host locomotion or tidal motions), which may be more commonly encountered [9]. In remora's case, long-term attachment is important for maintaining a reliable food source and locating mates [13, 19, 20], and its attachment strength exceeds the drag forces applied during sustained swimming by an order of magnitude [7, 26]. Detachment of the remora by the host requires extraordinary effort occasionally observed as erratic body bending or breaching behavior [14, 15, 18]. In such cases where large disruptive forces are seldom encountered and prolonged attachment is desired, the effectiveness of the seal and its ability to prevent leakage should be of primary concern.

In the following analysis, attachment site topology and the mechanical properties relevant to the soft seal are characterized. These two topics are brought together when formulating the multi-scaled model for predicting the flow rate across a soft seal. To demonstrate the model's effectiveness, an experimental apparatus is presented which measures the flow rate across a viscoelastic material in contact with a rough mating surface under the influence of a controllable pressure difference (simulating suction-based attachment conditions). The measured flow rates are compared to model predictions. Furthermore, the sealing effectiveness of a remora's suction pad in contact with sharkskin is investigated using the approach as a specific biological example.

MODELING

Contact Surface Topology

Given the broad range of topologies to which organisms attach, a simplified representation of the surface topology was sought to capture the most important features with respect to fluid motion across the sealing interface. Therefore, topology of the contact surface was reduced to the two component representation as seen in Figure 2a [27]. The characterizing components of the surface were the root mean square roughness, R_q, and upper cutoff wavelength, l, which when combined with Eq. (1)-(3) (where X, Y, and Z are spatial coordinates parameterized by u and v) produce a simple cosine surface that preserves the largest peaks and valleys which form the largest flow channels across the seal. These two parameters were useful given that they are readily established in surface metrology and they can be obtained directly from surface power spectrum data [11, 28]. Additionally, the periodic nature of the representation (e.g. an arbitrarily large surface can be represented by translating the surface by l in the X and Y directions) facilitated a multi-scaled modeling approach, which is discussed later.

$$X = ul \tag{1}$$
$$Y = vl \tag{2}$$
$$Z = R_q \left(\cos(2\pi u) + \cos(2\pi v) \right), \; u, v \in [0,1] \tag{3}$$
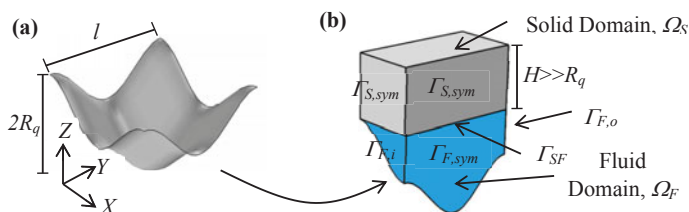

Figure 2. (a) Simplified contact surface and **(b)** cross section of unit cell showing solid and fluid domains

Viscoelastic Seal Properties

Soft materials such as natural tissues or manmade elastomers often exhibit time-dependent mechanical properties owing to their ability to both store and dissipate energy [29]. To account for this behavior viscoelastic constitutive laws are available, which in the linear case can be formed by discrete or continuous networks of rheological elements, or by more complex formulations in the nonlinear case [29, 30]. Here, time-dependent material properties were

accounted for with a linear viscoelastic constitutive model known as a Maxwell Model that is seen in Eq. (4), where t is time, $G(t)$ is the relaxation modulus, and G_0, k_n, and τ_n are fitting constants. Several studies attest to the suitability of this model to describe natural tissues [21, 31-36]. To implement Eq. (4) it was necessary to perform mechanical testing and obtain stress/strain data for the fitting constants.

$$G(t) = G_0 + \sum k_n e^{\frac{-t}{\tau_n}} \tag{4}$$

Multi-Scale Model Description

As discussed previously, the aim of the work is to predict the fluid flow rate across a sealing interface. The underlying idea behind multiple scale approach was that the microscopic channels, Figure 1d, created by the interface between the local topology and the soft material were small enough (less than an order of magnitude) to be considered infinitesimal when compared to the size of the seal, Figure 1c, but still of finite size such that the local microstructure exits [37, 38]. From this description, there are two length scales to consider, the local or micro-scale defined by the size of the flow channels, l in Eq. (1) and (2), and the global or macro-scale defined by the width of the seal, L. Under the assumption that $L >> l$, the seal was treated as sequentially solved solid mechanics and fluid dynamics unit cell problems that resulted in a relationship between seal permeability and deformation of the soft tissue with respect to local sub-ambient pressure changes [39, 40]. Locally, the sealing interface was discretized into individual unit cells, Figure 2b, with a prescribed local pressure to first determine the deformation of the solid and fluid domains. Then a prescribed local pressure gradient was applied to the deformed geometry to determine its permeability. Knowing the variation of permeability with respect to pressure, the volumetric flow rate across the seal was obtained with Darcy's Law [40].

The solid domain, Ω_S, was governed by Eq. (5)-(7) which represented the viscoelastic constitutive properties, strain tensor, and quasi-steady conservation of linear and angular momentum where T is the stress tensor, G is the relaxation modulus (Eq. (4), but as a tensor here), E is the strain tensor, u is the displacement vector, t is time, s is a dummy variable for integration, and x is the spatial coordinate vector [37]. The superscript T signifies transpose. The boundary conditions given in Eq. (8)-(9) represented the symmetry of the unit cell with adjacent cells on surfaces, $\Gamma_{S,sym}$, and the applied sub-ambient pressure at the fluid-solid interface, Γ_{SF}, where $\hat{n}$ is the surface unit normal vector and p_{avg} the prescribed pressure. The displacement of the fluid-solid interface was limited by a rigid contact surface based on the host topology, as described in the Contact Surface Topology section, using a penalty factor method [41, 42]. Here the need to provide continuity between the unit cells demonstrates the reasoning for a periodic representation of the contact surface. The height, H, of the solid domain was prescribed to be much greater than the surface roughness, R_q, such that no deformation of the top surface of occurred [43].

$$T(x,t) = \int_0^t G(t-s) \cdot \frac{DE}{Ds}(x,s)\,ds \tag{5}$$

$$E = \frac{1}{2}\left(\nabla u + (\nabla u)^{\mathrm{T}} + (\nabla u)^{\mathrm{T}}(\nabla u)\right) \tag{6}$$

$$\nabla \cdot T = 0, \ T^{\mathrm{T}} = T \tag{7}$$

$$\boldsymbol{u} \cdot \hat{\boldsymbol{n}} = 0 \text{ on } \Gamma_{S,sym} \tag{8}$$

$$\boldsymbol{T} \cdot \hat{\boldsymbol{n}} = -p_{avg}\hat{\boldsymbol{n}} \text{ on } \Gamma_{SF} \tag{9}$$

The fluid domain, Ω_F, was governed by Eq. (10)-(11), which represented steady, laminar, incompressible flow with v as the velocity vector, p as pressure, μ as viscosity, and I is the identity tensor. The boundary conditions in Eq. (12)-(14) represented "no slip" on the fluid-solid interfaces [44], Γ_{FS}, the prescribed pressure difference (p_i - p_o) between the cell inlet, $\Gamma_{F,i}$, and outlet, $\Gamma_{F,o}$, and symmetry on the remaining surfaces, $\Gamma_{F,sym}$, to maintain continuity between adjacent unit cells (Figure 2b).

$$\nabla \cdot \boldsymbol{v} = 0 \tag{10}$$

$$\rho\left(\boldsymbol{v}\cdot\nabla\right)\boldsymbol{v} = \nabla\cdot\left(-pI + \mu\left(\nabla\boldsymbol{v} + \left(\nabla\boldsymbol{v}\right)^{\mathrm{T}}\right)\right) \tag{11}$$

$$\boldsymbol{v} = 0 \text{ on } \Gamma_{FS} \tag{12}$$

$$p_i, p_o = \text{constants on } \Gamma_{F,i}, \Gamma_{F,o} \tag{13}$$

$$\boldsymbol{v}\cdot\hat{\boldsymbol{n}} = 0 \text{ on } \Gamma_{F,sym} \tag{14}$$

Once the fluid problem was solved, the relationship between the local volumetric flow, q, and the cell's permeability, K, was calculated from Darcy's Law as seen in Eq. (15) and (16).

$$q = \int_{\Gamma_{F,i}} \boldsymbol{v}\cdot\hat{\boldsymbol{n}}dS = \frac{K}{\mu}\left(\frac{p_i - p_o}{l}\right) \tag{15}$$

$$K\left(p_{avg}\right) = \mu\left(\frac{l}{p_i - p_o}\right)q \tag{16}$$

At the macro-scale (length scale of the seal, Figure 1c), Darcy's Law was again employed to solve for the volumetric flow rate across the entire seal, Q in Eq. (17), with K now a known function of pressure where L is the width of the seal and L_p is the perimeter of the seal.

$$Q = -\frac{KL_P}{\mu l}\frac{dp}{dx} = \frac{L_P}{\mu L l}\int_{p_i}^{p_o} Kdp \tag{17}$$

The model as outlined in the above equations can be solved numerically in commercially available finite element software. Here solution of the unit cell problems was carried out in Comsol Multiphysics (Version 4.3a, Stockholm, Sweden) with post-processing in MATLAB (R2009a, Natick, MA, USA).

MATERIALS AND METHODS

Contact Surface Topology

The contact surfaces studied were water-proof, 240 grit silicon carbide grinding paper (Allied High Tech Products, Rancho Dominguez, CA, USA) and the denticle surface of a Short Fin Mako Shark (*Isurus oxyrinchus*). The roughness, R_q, and wavelength, l, components of the grinding paper were obtained from its the power spectrum as computed by the Fast Fourier Transform technique in [11] using surface height data obtained from an Olympus LEXT 3D Material Confocal Microscope (Center Valley, PA, USA). In [21], the parameters for sharkskin were obtained in the same way where R_q, and l were found to be 10.5 and 200 μm, respectively.

Viscoelastic Seal Characterization

For validation, although the multi-scale model was conceived with biological applications in mind, a commercially available urethane elastomer (ReoFlex 30, Smooth-On Inc. Easton, PA, USA) rather than natural tissues was employed. This afforded several benefits with respect to reducing the uncertainty in material properties including guaranteed homogeneity, reduced dependence on hydration levels, and no confounding due to lack of homeostasis which are frequently cited as difficulties in working with biological tissues [21, 29, 31-37]. Furthermore, idealized geometries were also easily formed using an engineered material. Both relaxation test specimens and seals used in the permeability experiments on grinding paper were constructed by hand-mixing the two part urethane compound and casting the mixture into molds. The castings were allowed 48 hours to harden such that their full mechanical properties were obtained. Stress relaxation tests were carried out at room temperature (20°C) in accordance with [45] on three independently prepared 15 x 3.25 x 130 mm specimens using an ESM301 test frame equipped with an M5-20 force gauge (Mark-10, Copiague, NY, USA). Eq. (4) was then fit to the data in a least squared sense.

Characterization of remora fleshy lip tissue has been carried out in [21]. In the study, tissue was sectioned from the fleshy lip and characterized with compressive, uniaxial dynamic mechanical analysis (DMA). The Maxwell Model parameters are shown in Table I. Concerning the differences in testing methods, broadly speaking, relaxation tests are more suitable for observing material behavior at long time scales ($>10^1$ s) whereas DMA is more convenient for shorter time scales (10^{-10} to 10^5 s) [30], though there is an appreciable region of overlap.

Model Validation and Simulations

Validation of the interfacial permeability model was carried out using the experimental setup in Figure 3. The apparatus was designed to measure both the flow rate and sub-ambient pressure difference across the seal in contact with a rough surface to be comparable with model predictions. At the base of the device (Figure 3), a custom annular viscoelastic seal (ReoFlex 30 urethane rubber) with a 5x5 mm square cross section (L) and diameter of 45 mm (L_p ~14.1 cm) was bonded to a rigid member using epoxy. The member was adjusted via a threaded connection and electrical conductivity measurements such that the base of the seal was precisely flush with the base of the center tubing. This was to ensure that deformation of the seal was only due to movement of the fluid (water) across the interface and not due to compression of the seal by the reduced pressure under the member. Once aligned, the base of the center tube and seal were brought into contact with the rough substrate (240 grit grinding paper) and the vacuum source was activated along with a peristaltic pump that maintained a constant fluid height (pressure head) above the substrate. After steady state was achieved the pressure difference across the seal was measured with an electronic pressure transducer (Cole-Parmer Instrument Company Model 68075, Vernon Hills, IL, USA) and the flow rate was calculated using a graduated cylinder and stopwatch. The flow rate at several sub-ambient pressure differences spanning 0 to 20 kPa were obtained by manually adjusting the vacuum source with a pressure regulator. For comparison, the interfacial permeability model was solved over a sub-ambient pressure range of 1 Pa to 100 kPa using the properties of water at room temperature (20°C) in addition to the measured material properties of the viscoelastic seal and the topology of the rough substrate.
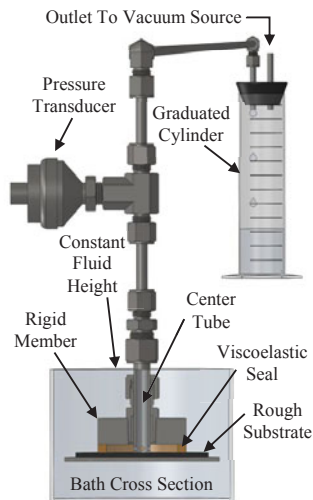
Figure 3. Interfacial permeability measurement system

      With respect to the remora on shark skin, the interfacial permeability model was solved over a sub-ambient pressure range of 1 to 300 Pa using the properties of water at room temperature (20°C). The perimeter of the remora pad was assumed to be 100 mm with a seal thickness of 3 mm. These values correspond to a remora approximately 19 cm in length as was observed when attached to a glass slide [21].

RESULTS

Contact Surface Topology

      The power spectrum of the rough substrate (240 grit grinding paper) is seen in Figure 4. The root mean square roughness, R_q, and cutoff wavelength, l, needed to characterize the surface in the multi-scaled model were 34.8 and 318 μm, respectively. The appropriateness of the cosine surface is reinforced by the exponential decay of the power spectrum, as from [11] it is known that the roughness of such surfaces is dominated by the cutoff wavelength as others fall off rapidly. Also, the ratio of the length of the seal, L (5 mm), to the cut-off wavelength, l, was approximately 16, meaning that the size of the unit cell was an order of magnitude smaller than the size of the seal, making the multi-scaled approach possible. These conditions were also satisfied by the sharkskin with a ratio of L (3 mm) to l (200 μm) of 15.
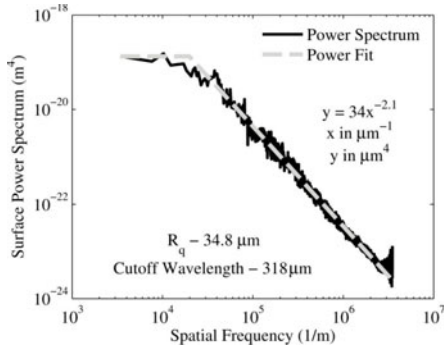
Figure 4. Power spectrum of rough surface (240 grit grinding paper) used in experimental permeability apparatus

<u>**Seal Viscoelastic Properties**</u>

The relaxation moduli and resulting Maxwell Material Model parameters are shown in Figure 5 and Table I. As expected, the modulus monotonically decreased with increasing time [30]. The leading order term (Young's Modulus) of the Maxwell Model was slightly lower than that expected for a rubber with a 30A Shore durometer (~1 MPa [46]), which was most likely due to the formation of bubbles resulting from the mixing process. However, the results were very consistent among independently prepared samples as there was negligible deviation (<5%) from the values in Table I.
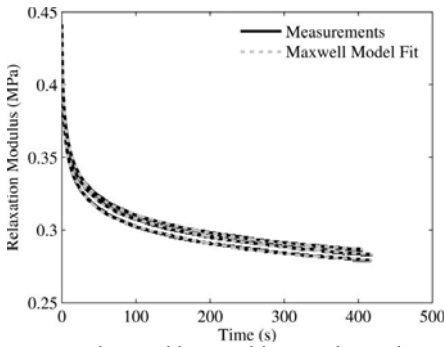

Figure 5. Relaxation tests on urethane rubber used in experimental permeability apparatus with accompanying Maxwell Material Model

2538

Table I. Average Maxwell Model fitting parameters for urethane rubber (ReoFlex 30) and remora fleshy lip tissue

Material	Property	Maxwell Element			Young's Modulus (kPa)	Poisson's Ratio
		1st	2nd	3rd		
Urethane Rubber (ReoFlex 30)	k (kPa)	49.00	57.05	46.14	277.4	0.495
	τ (s)	197.8	2.175	20.25		
Remora Tissue	k (Pa)	0.860	2.70	0.700	3.980	0.495
	τ (s)	0.11	0.016	0.68		

Model Results and Validation

An example of the displacement field magnitude resulting from solution of the solid mechanics unit cell problem is shown in Figure 6b for urethane rubber on grinding paper at 10 kPa sub-ambient pressure. Looking at the deformed configuration, it is possible to see how the soft rubber was displaced into the rough contact surface, and also how the deformed fluid domain was obtained from the space between. Figure 6c shows the velocity field magnitude corresponding to solution of the fluid mechanics unit cell problem at 10 kPa sub-ambient pressure with a prescribed pressure difference of 10 Pa across the unit cell (equal to a pressure gradient of 3.2×10^{-2} kPa/mm). Using the velocity field and Eq. (15) and (16), the permeability of the deformed cell was calculated at different pressure gradients (Figure 6a). It can be seen that the local permeability of the deformed cell was constant with respect to the pressure gradient below approximately 10 kPa/mm, which is a necessary condition for application of the model (Darcy's Law).
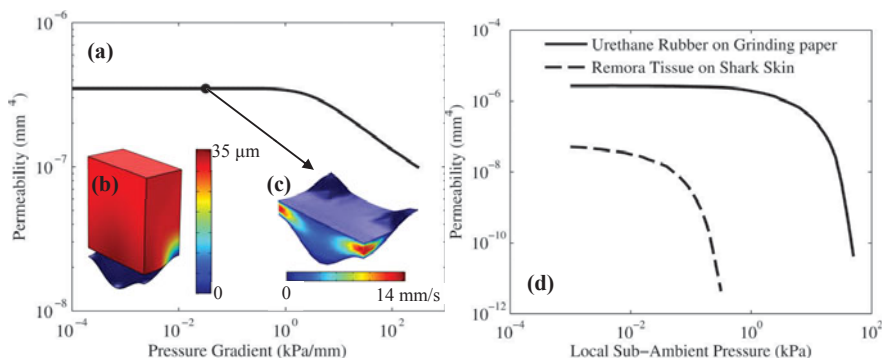

Figure 6. (a) Cell permeability at 10 kPa sub-ambient pressure vs. pressure gradient; and corresponding **(b)** solid domain displacement magnitude and **(c)** fluid domain velocity magnitude. **(d)** Permeability of seals vs. local sub-ambient pressure

Repeated solution of the cell problems over a sub-ambient pressure range spanning 1 Pa to 100 kPa in the urethane rubber case and 1 to 300 Pa in the case of the remora on shark skin resulted in their respective pressure dependent interfacial permeabilities, K (Figure 6d). In both cases, at low sub-ambient pressures the permeability achieved its largest value and remained nearly constant, but as the sub-ambient pressure gradually increased, the permeability began to

fall rapidly after approximately 1 kPa for the urethane rubber on grinding paper and 30 Pa for the remora tissue on shark skin. Integration of the permeabilities using Eq. (17) yielded estimates of the expected flow rates across the seals. The expected flow rate of the urethane seal against grinding paper for sub-ambient pressure differentials ranging between 0 and 20 kPa is shown in Figure 7a along with flow rate measurements made on the permeability test apparatus. Similarly, the expected flow rate into the remora's dorsal pad during attachment to shark skin at sub-ambient pressure differentials from 0 to 300 Pa is shown in Figure 7b. In both cases flow rates increased at a decreasing rate with respect to increasing sub-ambient pressure differences. Furthermore, in the case of the urethane seal, reasonable agreement was obtained between the predicted and measured values.
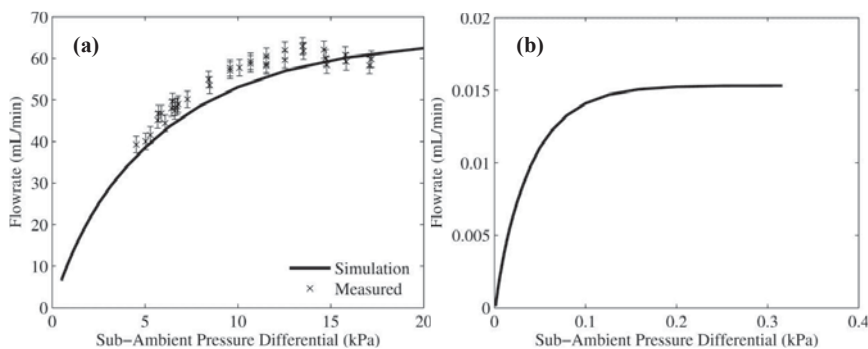

Figure 7. Model simulation results and flow rate tests using experimental permeability apparatus **(a)** and model simulation results for remora pad **(b)**

DISCUSSION

There are several important implications from the model. First, it provides some explanation as to how a cutaneous mucus layer could significantly improve an organism's sealing effectiveness, and, therefore, provide an important contribution to a suction-based attachment strategy. Many marine animals, including remoras [47], are known to secrete mucus with unique properties [5, 48]. Looking at Eq. (17) one can see the advantage of a mucus that increases the viscosity of the surrounding fluid environment, as this reduces fluid flow across the seal. Measurement of mucus secretions from salmonids (teleost fish, as are remora) has shown significant increases in viscosity by as much as 5 to 10 times that of clean water [49]. Such increases in fluid viscosity should have a strong impact on sealing effectiveness. In addition to viscous effects, Eq. (17) also shows several geometric parameters of the seal that can linearly alter the flow rate including widening the seal and reducing its perimeter. These too are therefore important design parameters for suction based devices.

To the extent that material properties play a role in improving the seal, the model demonstrates the advantage of having softer more conformal tissues at the sealing interface. Figure 6d shows a dramatic drop in the permeability of the interface at increasing sub-ambient pressures beyond approximately 1 kPa for the urethane rubber on grinding paper and 30 Pa for the remora tissue on shark skin. This is a result of the sealing material being drawn into the rough substrate and restricting flow as seen in Figure 6b. Since deformation of the seal is directly

proportional to its stiffness from Eq. (5), it follows that the onset of the drop in permeability, and therefore reduced flow rates over an increased pressure range, will occur at lower sub-ambient pressures for softer vs. harder sealing materials. This translates into reduced leakage, which facilitates prolonged suction-based attachment. In practice, a softer contact interface may be achieved by bonding softer materials to the contact surface, for example.

When considering the bottom-up, multi-scaled approach taken here, one can see how the model presented is not limited to a particular species in terms of its application. Rather, the basic geometric, material, fluid, and topological properties of the materials and structures involved drive the analysis. In turn, this approach could be applied to a variety of organismal or manmade systems with the appropriate structural, topological, and material properties.

CONCLUSION

In this work, a model of interfacial permeability was presented to estimate the leakage rate associated with suction based attachment in marine organisms. The model was based on fundamental material and transport properties of the fluids and structures involved, and also the attachment site topology and geometry. The effectiveness of the model was demonstrated by direct measurements on an artificial suction seal and through its application to the remora fish. Several important factors were identified as crucial to a suction based attachment strategy including the importance of a cutaneous mucus layer, the roughness of the attachment site, and the softness of the seal material.

REFERENCES

1. Czernik, D.E., *Internal Combustion Engine Gaskets*, in *Gaskets and Gasketed Joints*, J.H. Bickford, Editor. 1997, Marcel Dekker, Inc.: New York, NY.
2. Fisher, E.W., *Packing and Seals*, in *Marks' Standard Handbook for Mechanical Engineers*, E.A. Avallone and T.B. III, Editors. 1987, McGraw-Hill Inc.: New York, NY.
3. Wainwright, D.K., et al., *Stick tight: suction adhesion on irregular surfaces in the northern clingfish.* Biology Letters, 2013. **9**(3).
4. Ditsche, P., D.K. Wainwright, and A.P. Summers, *Attachment to challenging substrates – fouling, roughness and limits of adhesion in the northern clingfish (Gobiesox maeandricus).* The Journal of Experimental Biology, 2014. **217**(14): p. 2548-2554.
5. Byern, J.v. and I. Grunwald, *Biological Adhesive Systems*. 2010, New York: Springer Science.
6. Smith, A.M., *Cephalopod sucker design and the physical limits to negative pressure.* Journal of Experimental Biology, 1996. **199**(4): p. 949-958.
7. Fulcher, B.A. and P.J. Motta, *Suction disk performance of echeneid fishes.* Canadian Journal of Zoology-Revue Canadienne De Zoologie, 2006. **84**(1): p. 42-50.
8. Davenport, J. and V. Thorsteinsson, *Sucker Action in the Lumpsucker Cyclopterus-Lumpus L.* Sarsia, 1990. **75**(1): p. 33-42.
9. Gibson, R.N., *Powers of adhesion in Liparis montagui (Donovan) and other shore fish.* Journal of Experimental Marine Biology and Ecology, 1969. **3**(2): p. 179-190.
10. De Meyer, J. and T. Geerinckx, *Using the Whole Body as a Sucker: Combining Respiration and Feeding with an Attached Lifestyle in Hill Stream Loaches (Balitoridae, Cypriniformes).* Journal of Morphology, 2014. **275**(9): p. 1066-1079.

11. Persson, B.N.J., et al., *On the nature of surface roughness with application to contact mechanics, sealing, rubber friction and adhesion.* Journal of Physics-Condensed Matter, 2005. **17**(1): p. R1-R62.

12. Persson, B.N.J. and C. Yang, *Theory of the leak-rate of seals.* Journal of Physics-Condensed Matter, 2008. **20**(31).

13. Strasburg, D.W., *Some Aspects of the Feeding Behavior of Remora remora.* Pacific Science, 1962. **16**(2): p. 202-206.

14. Ritter, E.K., *Analysis of sharksucker, Echeneis naucrates, induced behavior patterns in the blacktip shark, Carcharhinus limbatus.* Environmental Biology of Fishes, 2002. **65**(1): p. 111-115.

15. Ritter, E.K. and J.M. Brunnschweiler, *Do Sharksuckers, Echeneis naucrates, Induce Jump Behaviour in Blacktip Sharks, Carcharhinus limbatus?* Marine and Freshwater Behaviour and Physiology, 2003. **36**(2): p. 111-113.

16. Williams Jr, E.H., et al., *Echeneid–sirenian associations, with information on sharksucker diet.* Journal of Fish Biology, 2003. **63**(5): p. 1176-1183.

17. Sazima, I. and A. Grossman, *Turtle riders: remoras on marine turtles in Southwest Atlantic.* Neotropical Ichthyology, 2006. **4**(1): p. 123-126.

18. Weihs, D., F.E. Fish, and A.J. Nicastro, *Mechanics of Remora Removal by Dolphin Spinning.* Marine Mammal Science, 2007. **23**(3): p. 707-714.

19. Silva-Jr, J.M. and I. Sazima, *Whalesuckers and a spinner dolphin bonded for weeks: does host fidelity pay off?* Biota Neotropica, 2003. **3**(2): p. 1-5.

20. Cressey, R.F. and E.A. Lachner, *The parasitic copepod diet and life history of diskfishes (Echeneidae).* Copeia, 1970. **1970**(2): p. 310-318.

21. Culler, M., K.A. Ledford, and J.H. Nadler. *The role of topology and tissue mechanics in remora attachment*. in *MRS Fall Meeting 2013*. 2013. Boston, MA.

22. Nadler, J.H., et al. *Structures and Function of Remora Adhesion*. in *MRS Spring Meeting 2013*. 2013. San Fransisco, CA.

23. Kier, W.M. and A.M. Smith, *The structure and adhesive mechanism of octopus suckers.* Integrative and Comparative Biology, 2002. **42**(6): p. 1146-1153.

24. Persson, B.N.J., et al., *Contact area between a viscoelastic solid and a hard, randomly rough, substrate.* The Journal of Chemical Physics, 2004. **120**(18): p. 8779-8793.

25. Chen, P.Y., J. McKittrick, and M.A. Meyers, *Biological materials: Functional adaptations and bioinspired designs.* Progress in Materials Science, 2012. **57**(8): p. 1492-1704.

26. Beckert, M., B.E. Flammang, and J.H. Nadler, *Theoretical and computational fluid dynamics of an attached remora (Echeneis naucrates)*. 2014.

27. Beckert, M., B.E. Flammang, and J.H. Nadler, *Remora fish suction pad attachment is enhanced by spinule friction.* Journal of Experimental Biology, 2015. **218**(22): p. 3551-3558.

28. Vorburger, T.V., *Methods for Characterizing Surface Topology*. Tutorials in Optics: Osa Annual Meeting, Rochester NY, ed. D.T. Moore. 1992, Washington DC: Optical Society of America.

29. Fung, Y.C., *Biomechanics Mechanical Properties of Living Tissues*. 1993: Springer-Verlag New York Inc.

30. Lakes, R.S., *Viscoelastic Solids*. 1999, Boca Raton, FL: CRC Press.

31. Krouskop, T.A., et al., *Elastic moduli of breast and prostate tissues under compression.* Ultrasonic Imaging, 1998. **20**(4): p. 260-274.

32. Guarnieri, F.A. and A. Cardona, *3D Solid Incompressible Viscoelastic Finite Element in Large Strains for the Cornea.* Mechanica Computacional, 1997. **18**: p. 799-808.

33. Liu, Z. and L. Bilston, *On the viscoelastic character of liver tissue: experiments and modelling of the linear behaviour.* Biorheology, 2000. **37**(3): p. 191-201.

34. Kiss, M.Z., T. Varghese, and T.J. Hall, *Viscoelastic characterization of in vitro canine tissue.* Physics in Medicine and Biology, 2004. **49**(18): p. 4207-4218.

35. Haghpanahi, M. and H.A. Naeeni. *Investigation of Viscoelastic Properties of Human Liver Tissue Using MR Elastography and FE Modeling*. in *Proceedings of the 17th Iranian Conference of Biomedical Engineering*. 2010.

36. Chatelin, S., et al., *In vivo liver tissue mechanical properties by transient elastography: Comparison with dynamic mechanical analysis.* Biorheology, 2011. **48**(2): p. 75-88.

37. Cowin, S.C. and S.B. Doty, *Tissue Mechanics*. 2007: Springer Science.

38. Biot, M.A., *General theory of three-dimensional consolidation.* Journal of Applied Physics, 1941. **12**(2): p. 155-164.

39. Mei, C.C. and B. Vernescu, *Homogenization Methods for Multiscale Mechanics*. 2010, 27 Warren St, Suite 401-402, Hackensack, NJ 07601: World Scientific Publishing Co.Pte.Ltd.

40. Dullen, F.A.L., *Porous Media Fluid Transport and Pore Structure*. 2nd ed. 1992, Sandiago, CA: Academic Press Inc.

41. Hallquist, J.O., G.L. Goudreau, and D.J. Benson, *Sliding interfaces with contact-impact in large-scale Lagrangian computations.* Computer Methods in Applied Mechanics and Engineering, 1985. **51**(1–3): p. 107-137.

42. Belytschko, T., W.K. Liu, and B. Moran, *Nonlinear Finite Elements for Continua and Structures*. 2000: Wiley.

43. Hyun, S., et al., *Finite-element analysis of contact between elastic self-affine surfaces.* Physical Review E, 2004. **70**(2).

44. Anderson, E.J., W.R. McGillis, and M.A. Grosenbaugh, *The boundary layer of swimming fish.* Journal of Experimental Biology, 2001. **204**(1): p. 81-102.

45. ASTM, *Standard Practice for Stress Relaxation Testing of Raw Rubber, Unvulcanized Rubber Compounds, and Thermoplastic Elastomers*. 2012, ASTM International: West Conshohocken, PA.

46. Mix, A.W. and A.J. Giacomin, *Standardized Polymer Durometry.* Journal of Testing and Evaluation, 2011. **39**(4): p. 696-705.

47. Sewell, R.B.S., *The adhesive apparatus of the " sucking-fish ".* Nature, 1925. **115**: p. 48-49.

48. Shephard, K.L., *Functions for Fish Mucus.* Reviews in Fish Biology and Fisheries, 1994. **4**(4): p. 401-429.

49. Roberts, S.D. and M.D. Powell, *The viscosity and glycoprotein biochemistry of salmonid mucus varies with species, salinity and the presence of amoebic gill disease (vol 175, pg 1, 2004).* Journal of Comparative Physiology B-Biochemical Systemic and Environmental Physiology, 2005. **175**(3): p. 219-219.